Electronic Supplementary Material (ESI) for Chemical Communications.

Toroidal versus centripetal arrangement of the magnetic moment in a Dy_4 tetrahedron

Qianqian Yang, Liviu Ungur, Liviu F. Chibotaru and Jinkui Tang**

Experimental Section

General Synthetic Considerations. All chemicals and solvents were commercially obtained and used as received without any further purification. FTIR spectra were measured using a Nicolet 6700 Flex FTIR spectrometer equipped with smart iTR™ attenuated total reflectance (ATR) sampling accessory in the range from 500 to 4000 cm^{-1}. Elemental analyses for C, H, and N were carried out on a Perkin-Elmer 2400 analyzer.

Synthesis of **Dy_4**: The complex has been synthesized by a typical "one-pot" strategy in which the ligand HL is generated in situ. A mixture of $Dy(NO_3)_3 \cdot 6H_2O$ (0.1 mmol), 2-hydrazino benzothiazole (0.1 mmol), *o*-vanillin (0.1 mmol), methanol (10 ml), and Et_3N (0.3 mmol) was sealed in a glass vial (20 ml, capacity) and the solution was heated at 90 °C for 1 h under autogenous pressure. After the mixture was allowed to cool to room temperature (12 h), yellow block single crystals were isolated from the vial. Yield: 39.2 mg, (73.7%, based on metal salt). Elemental analysis (%) calcd for $[Dy_4(\mu_4\text{-}O)L_2(HL)_2(CH_3O)_4] \cdot 4CH_3OH \cdot H_2O$ ($C_{68}H_{76}Dy_4N_{12}O_{18}S_4$, MW = 2127.64): C, 38.39, H, 3.6, N, 7.9; found C, 37.84, H, 3.47, N, 8.06. IR (solid, ATR) $\tilde{\upsilon}$ [cm^{-1}] = 3192 (br), 2939 (w), 2802 (w), 1605 (s), 1553 (m), 1521 (m), 1492 (m), 1452 (s), 1386 (s), 1313 (w), 1292 (w), 1256 (m), 1215 (s), 1167 (s), 1131 (w), 1102 (m), 1080 (w), 1067 (m), 973 (m), 933 (m), 859 (w), 823 (w), 741 (m), 671 (w), 634 (w), 557 (m), 471 (w), 415 (m).

Crystallography

Single-crystal X-ray data of the titled complex was collected on a Bruker Apex II CCD diffractometer equipped with graphite-monochromatized Mo-Kα radiation (λ = 0.71073 Å) at 273 K. The structures were solved with SHELXT and refined on *F*2 using all reflections with ShelXL[1] (full-matrix least-squares techniques) in the Olex2 package.[2] All non-hydrogen atoms in the whole structure were refined with anisotropic displacement parameters. Hydrogen atoms were introduced in calculated positions and refined with fixed geometry with respect to their carrier atoms. The empirical formula and derived values are in accordance with the calculated cell content. Crystallographic data are listed in Table S1. CCDC 2117123 contains the supplementary crystallographic data for this paper. These data can be obtained free of charge from the Cambridge Crystallographic Data Centre via www.ccdc.cam.ac.uk/data_request/cif.

Magnetic Measurements

Magnetic susceptibility measurements were recorded on a Quantum Design MPMS-XL7 SQUID magnetometer equipped with a 7 T magnet. Direct current (dc) magnetic susceptibility measurements were performed on a polycrystalline sample of **Dy_4** in the temperature range 2–300 K, in an applied field of 1000 Oe. The field-dependent magnetizations for all complexes were measured in the field range of 0−7 T. The dynamics of the magnetization were investigated from the ac susceptibility measurements in the zero static fields and a 3.0 Oe ac oscillating field. Diamagnetic corrections were made with Pascal's constants for all the constituent atoms as well as the contributions of the sample holder.[3]

Table S1 Crystallographic data of complex **Dy_4**.

	Dy_4
Formula	$C_{68}H_{76}Dy_4N_{12}O_{18}S_4$
FW, g·mol^{-1}	2127.64
crystal system	Monoclinic
space group	*C2/c*
T, K	273.15
λ, Å	0.71073
a, Å	18.9036(9)
b, Å	22.8201(11)
c, Å	18.1253(9)
α, °	90
β, °	90.2630(10)
γ, °	90
V, Å^3	7818.8(7)
Z	4
ρ_{calcd}, g·cm^{-3}	1.806
F(000)	4151.9
2θ range [°]	3.57 to 52.37
Tmax / Tmin	0.471 / 0.490
measured refl.	21682
unique refl. [Rint]	7818, 0.0535
goodness-of-fit (F^2)	1.005
data / restr. / param.	7818 / 0 / 489
R1, wR2 (I > 2σ(I))	0.0378, 0.0756
R1, wR2 (all data)	0.0550, 0.0821
res. el. dens. [e·Å^{-3}]	0.97 / -0.61

Table S2 Selected bond distances (Å) and angles of complex **Dy_4**.

Dy1-N1	2.524(4)	Dy2-N4	2.545(5)	Dy1$^{\#}$-O1-Dy1	104.71(19)
Dy1-N3	2.460(5)	Dy2-N6	2.472(5)	Dy1$^{\#}$-O1-Dy2	112.007(10)
Dy1-O1	2.177(3)	Dy2-O1	2.187(3)	Dy1$^{\#}$-O1-Dy2$^{\#}$	111.887(10)
Dy1-O2$^{\#}$	2.573(4)	Dy2-O4$^{\#}$	2.567(4)	Dy1-O1-Dy2	111.886(10)
Dy1-O3$^{\#}$	2.507(4)	Dy2-O5$^{\#}$	2.489(4)	Dy1-O1-Dy2$^{\#}$	112.010(10)
Dy1-O3	2.352(4)	Dy2-O5	2.351(3)	Dy2-O1-Dy2$^{\#}$	104.53(18)
Dy1-O6	2.275(4)	Dy2-O6	2.317(3)	O6-Dy2-O5$^{\#}$	135.94(12)
Dy1-O7$^{\#}$	2.333(4)	Dy2-O7	2.271(4)	O7-Dy2-O5	139.80(14)
Dy1-Dy1$^{\#}$	3.4473(5)	Dy2-Dy1$^{\#}$	3.6181(4)	O7-Dy2-O6	108.02(12)
Dy1-Dy2	3.6156(4)	Dy2-Dy2$^{\#}$	3.4598(6)	O6-Dy1-O3	140.02(13)
				O6-Dy1-O7$^{\#}$	109.20(13)
				O7$^{\#}$-Dy1-O3$^{\#}$	135.75(13)

$^{\#}$1-X,+Y,1/2-Z

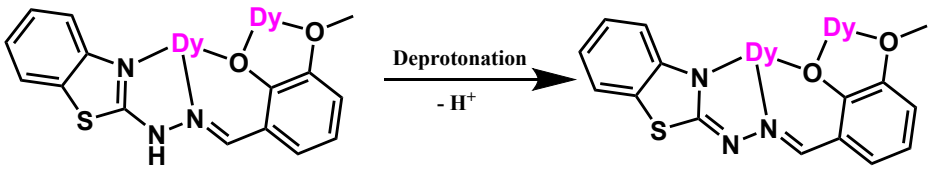

Scheme S1 Schematic drawing of the once (left) and twice (right) deprotonated ligands in the complex.

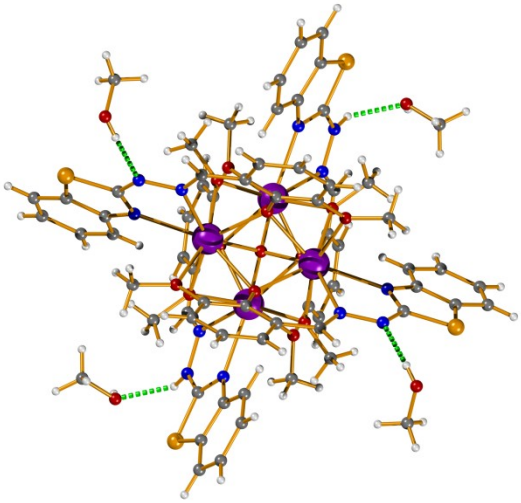

Fig. S1 Structure view of complex **Dy_4** along *b* axis with purple, blue, grey, white, orange, and red spheres representing Dy, N, C, H, S, and O, respectively; some solvents have been omitted for clarity. The green dash lines represent the hydrogen bondings.

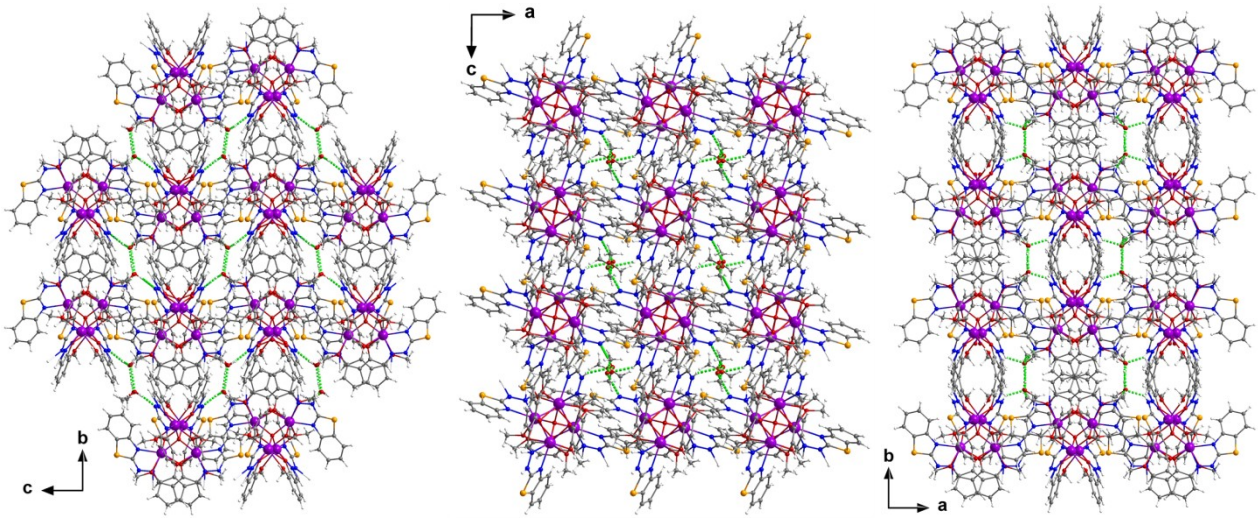

Fig. S2 Packing models along *a*, *b*, and *c* axes of complex **Dy_4** with purple, blue, grey, white, orange, and red spheres representing Dy, N, C, H, S, and O, respectively. The green dash lines represent the hydrogen bondings.

Table S3 The *CShM* values calculated by *SHAPE* 2.1 for **Dy_4**.

Central atom	Coordination Geometry	Dy1	Dy2
Dy	Cube (O_h)	9.851	9.968
	Square antiprism (D_{4d})	1.720	1.759
	Triangular dodecahedron (D_{2d})	2.980	3.103
	Johnson gyrobifastigium J26 (D_{2d})	14.135	14.307
	Johnson elongated triangular bipyramid (D_{3h})	25.957	26.288
	Biaugmented trigonal prism (C_{2v})	2.750	2.918
	Snub diphenoid J84 (D_{2d})	4.735	5.021

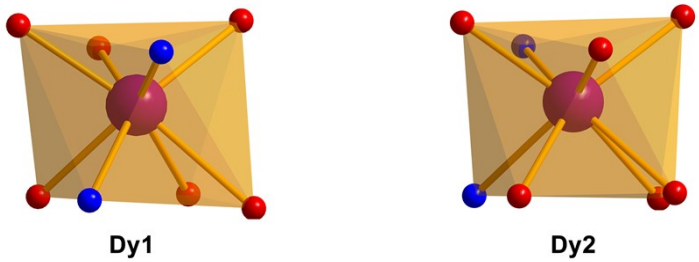

Fig. S3 Coordination polyhedrons of Dy1 (left) and Dy2 (right) in complex **Dy_4**.

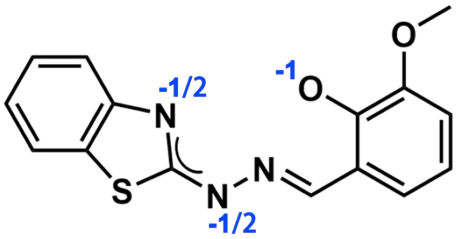

Fig. S4 Partial charges assigned to the formally ligand in complex **Dy_4**.

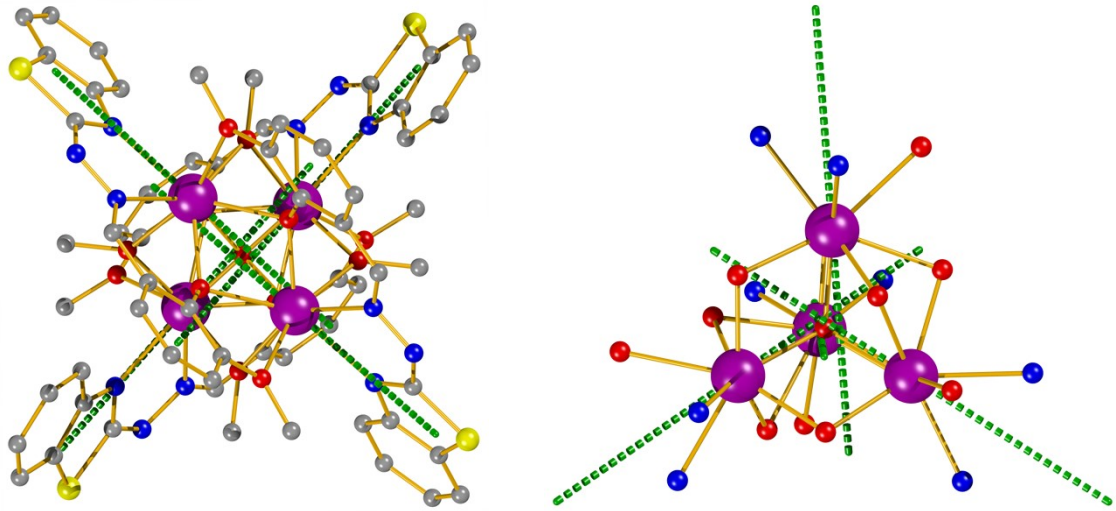

Fig. S5 Ground-state magnetic anisotropy in the molecule (left) and the relevant magnetic anisotropy orientations in Dy_4 core (right) of complex **Dy_4**. The green dash lines represent the orientations of the anisotropic axes for each Dy^{III} ion, as calculated by the electrostatic model.

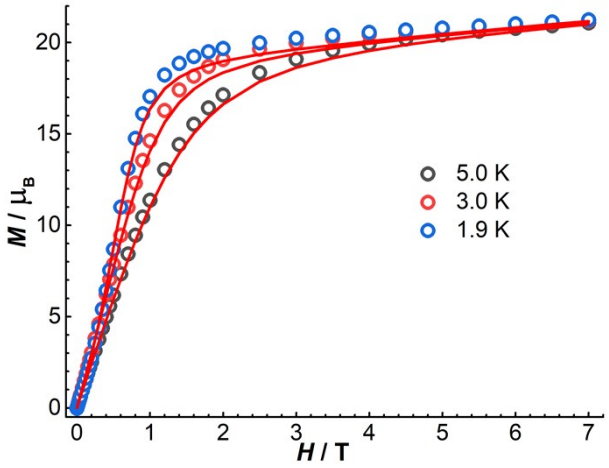

Fig. S6 Molar magnetization (*M*) *vs*. *H* for **Dy$_4$** at 1.9, 3.0, and 5.0 K. The red lines represent the calculation results.

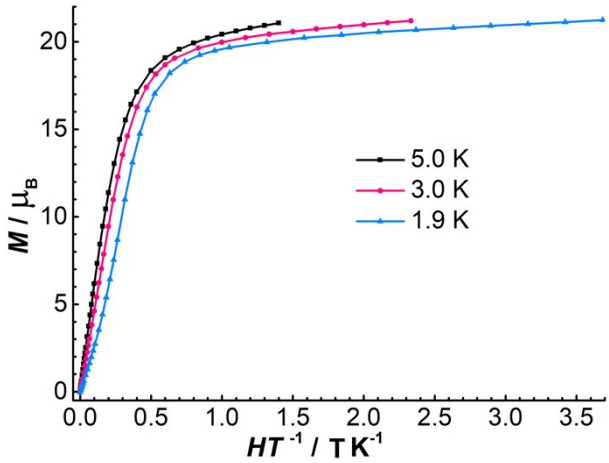

Fig. S7 Molar magnetization (*M*) *vs*. *H*/*T* for **Dy$_4$** at 1.9, 3.0, and 5.0 K.

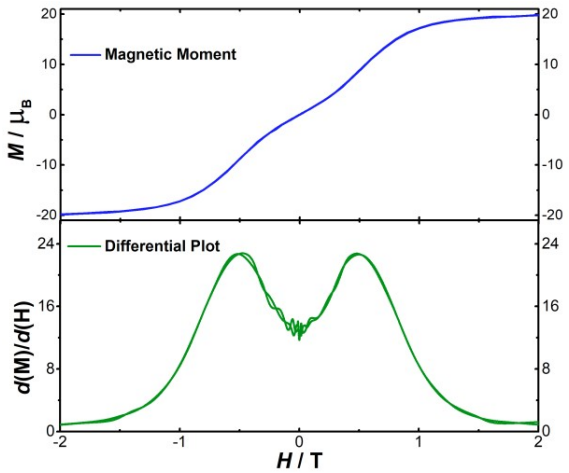

Fig. S8 Field-dependent magnetic moment (top) and the relevant differential plot (bottom) of **Dy$_4$** at 1.9 K.

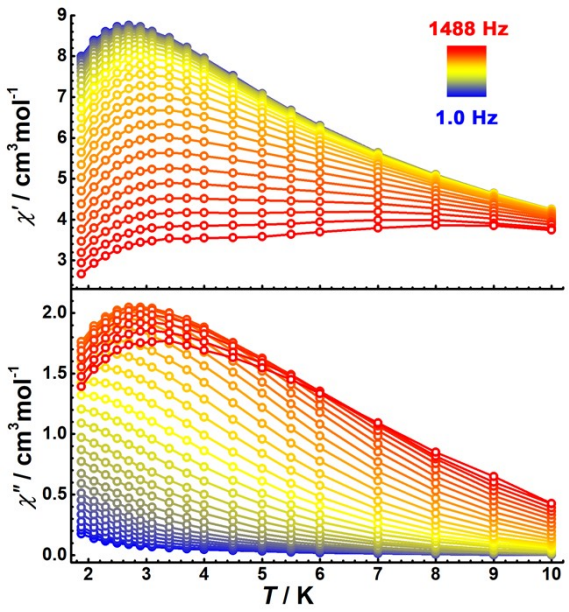

Fig. S9 Temperature-dependent ac susceptibility for **Dy_4** at indicated frequencies under zero dc field.

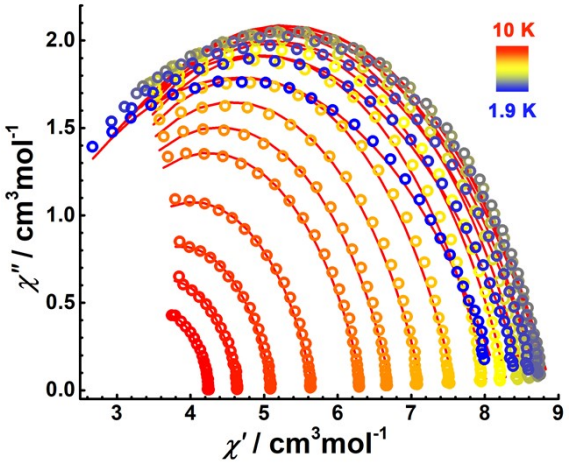

Fig. S10 Cole-Cole plots for **Dy_4** at zero field between 1.9 and 10 K. The solid lines indicate the best fits.

Table S4. The best fit of frequency-dependent ac susceptibility of **Dy_4** under zero dc field.

T / K	χ_S	χ_T	τ / s	α	*Residual*
10	3.05747	4.25431	6.98266E-5	0.20362	0.00574
9	2.77786	4.65446	9.33179E-5	0.24941	0.01223
8	2.64239	5.11417	1.20528E-4	0.2518	0.01662
7	2.41162	5.66787	1.51041E-4	0.25584	0.02629
6	2.16912	6.34176	1.92256E-4	0.26511	0.04457
5.5	2.05888	6.72586	2.17302E-4	0.27044	0.05798
5	1.98422	7.14875	2.47967E-4	0.27629	0.07458
4.5	1.93755	7.59079	2.81254E-4	0.28229	0.09218
4	1.8895	8.04819	3.1489E-4	0.29226	0.10901
3.7	1.84571	8.31913	3.34674E-4	0.29996	0.11296
3.4	1.79977	8.56545	3.54506E-4	0.30962	0.12458

3.1	1.70756	8.73629	3.72729E-4	0.32262	0.1256
2.9	1.69529	8.85667	3.965E-4	0.32807	0.11392
2.7	1.61233	8.89935	4.16029E-4	0.3384	0.10429
2.5	1.51713	8.87692	4.41491E-4	0.35124	0.09577
2.3	1.39118	8.76199	4.77491E-4	0.36732	0.07524
2.1	1.24955	8.56935	5.20648E-4	0.38556	0.05684
1.9	1.07871	8.22899	5.94407E-4	0.4095	0.044

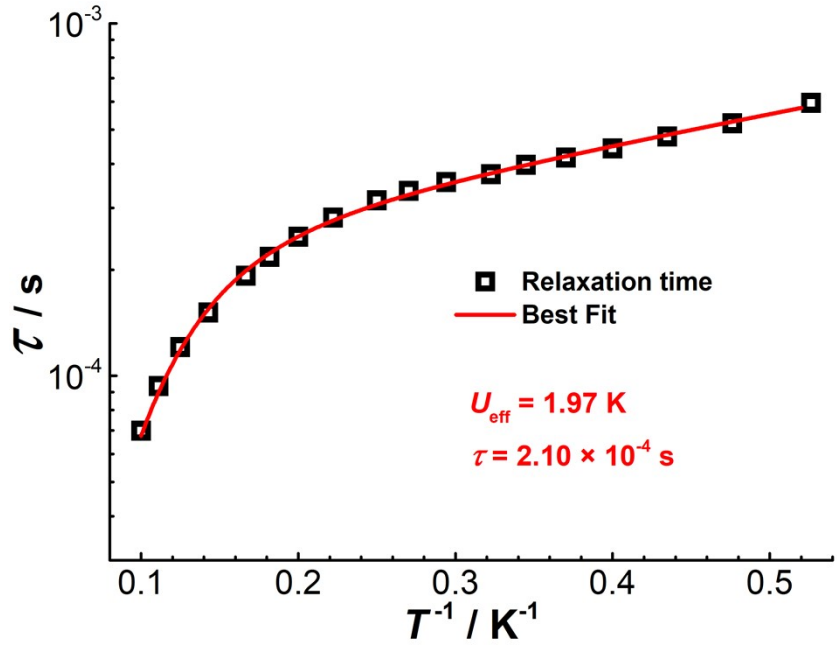

Fig. S11 Plot of τ *vs*. T^{-1} for **Dy$_4$** obtained under zero dc fields over the temperature range 1.9–10 K. The red line represents the best-fitted result.

Ab initio calculation on individual lanthanide fragment

All calculations were done with OpenMOLCAS (master version of 08 July 2021) and are of CASSCF/RASSI/SINGLE_ANISO type.[4] The mononuclear Dy^{III} fragments have the same structure as the initial **Dy_4** complex, in which all other three Dy ions were computationally substituted by diamagnetic Lu. DZP basis sets approximations have been employed. Active space of the CASSCF method included 9 electrons in 7 orbitals for Dy (4f orbitals of Dy^{III} ion). To exclude all the doubts, we calculated all the roots in the active space. The state-averaged CASSCF orbitals of the sextets, quartets, and doublets were optimized with 21, 224, and 490 states, respectively. We have mixed the maximum number of spin-free states which was possible with our hardware. On the basis of the resulting spin-orbital multiplets, SINGLE_ANISO program computed local magnetic properties (g-tensors, magnetic axes, local magnetic susceptibility, etc.). The magnetic properties of the entire complex, involving four Dy^{III} centers were calculated by the POLY_ANISO program, in which the anisotropic exchange interactions were simulated within the Lines model.[5]

Table S5 Energies (cm^{-1}) and *g* tensors of the lowest Kramers doublets (KD) on individual Dy^{III} ions.

KD		Dy1		Dy2		Dy1`		Dy2`	
		E	*g*	E	*g*	E	*g*	E	*g*
1	g_X		0.0080		0.0568		0.0080		0.0568
	g_Y	0.000	0.0189	0.000	0.1659	0.000	0.0189	0.000	0.1659
	g_Z		19.5032		18.3020		19.5032		18.3020
2	g_X		0.0807		0.1114		0.0807		0.1114
	g_Y	76.902	0.1673	46.262	0.2741	76.885	0.1673	46.262	0.2741
	g_Z		19.0440		16.5280		19.0440		16.5280
3	g_X		0.7951		1.7246		0.7951		1.7246
	g_Y	143.492	1.0665	151.754	2.4218	143.490	1.0665	151.754	2.4218
	g_Z		16.3288		14.0092		16.3288		14.0092
4	g_X		2.3590		0.2949		2.3590		0.2949
	g_Y	199.221	3.4409	186.842	1.6269	199.214	3.4409	186.842	1.6269
	g_Z		12.1360		14.6852		12.1360		14.6852
5	g_X		8.2544		2.2936		8.2544		2.2936
	g_Y	260.383	6.1164	223.587	4.2689	260.374	6.1164	223.586	4.2689
	g_Z		2.0996		9.0353		2.0996		9.0353
6	g_X		0.7727		2.4911		0.7727		2.4911
	g_Y	330.673	4.4454	261.827	4.6264	330.659	4.4454	261.827	4.6264
	g_Z		10.0012		11.8834		10.0012		11.8834
7	g_X		1.3283		0.1375		1.3283		0.1375
	g_Y	363.065	5.1869	366.232	0.1991	363.046	5.1869	366.232	0.1991
	g_Z		14.8360		18.9947		14.8360		18.9947
8	g_X		0.0106		0.0214		0.0106		0.0214
	g_Y	551.766	0.0210	505.620	0.0506	551.764	0.0210	505.620	0.0506
	g_Z		19.6880		19.6637		19.6880		19.6637

Table S6 Energies of the lowest spin-orbit states (cm^{-1}).

spin-orbit states (cm^{-1})			
Dy1	Dy2	Dy1`	Dy2`
0.000	0.000	0.000	0.000
76.902	46.262	76.885	46.262
143.492	151.754	143.490	151.754
199.221	186.842	199.214	186.842
260.383	223.587	260.374	223.586
330.673	261.827	330.659	261.827
363.065	366.232	363.046	366.232
551.766	505.620	551.764	505.620

Table S7 Angles between the main magnetic axes corresponding to the ground Kramers doublets on Dy centers (degrees).

	Dy1	Dy2	Dy1`	Dy2`
Dy1	0.000	55.008	63.103	82.315
Dy2	55.008	0.000	82.315	85.025
Dy1`	63.103	82.315	0.000	55.008
Dy2`	82.315	85.025	55.008	0.000

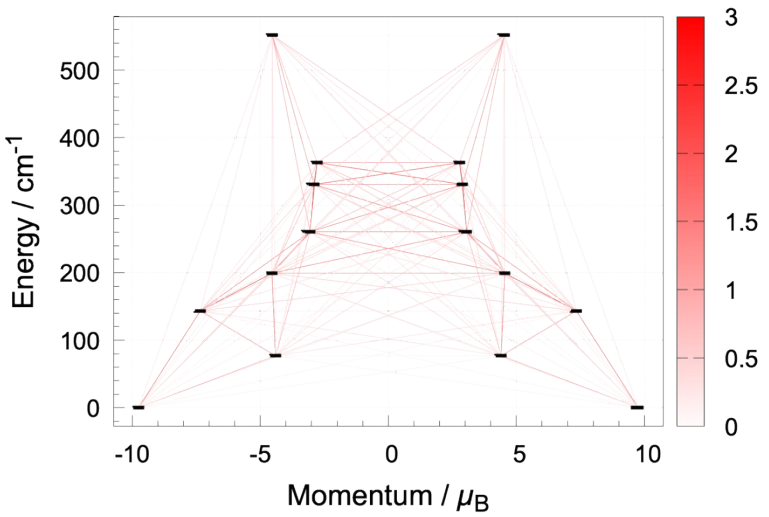

Fig. S12 Energy *vs*. momentum for the ground J =15/2 of Dy1 site. The intensity of the red lines indicates the amplitude of the average transition magnetic dipole moment in μ_B between the connected states (see the legend in the right-hand side), the square of which roughly scales with the rate of spin-phonon transition between them. The most intense lines outline the magnetization blocking barrier (solid red lines).

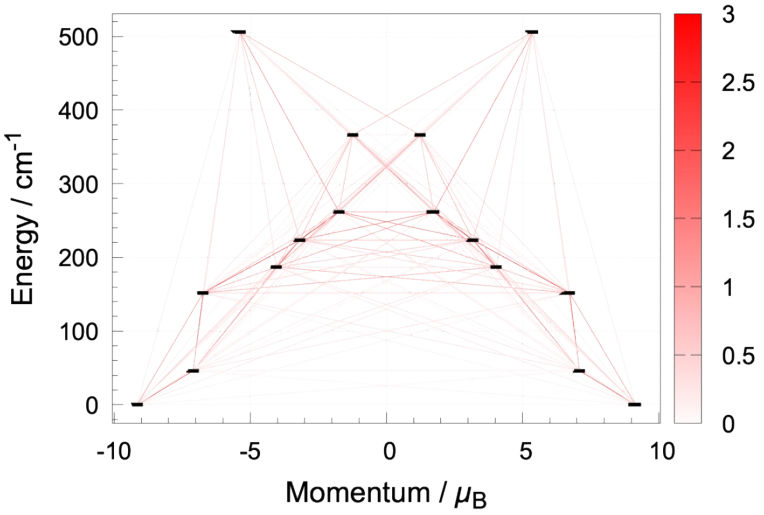

Fig. S13 Energy *vs*. momentum for the ground J =15/2 of Dy2 site. The intensity of the red lines indicates the amplitude of the average transition magnetic dipole moment in μ_B between the connected states (see the legend in the right-hand side), the square of which roughly scales with the rate of spin-phonon transition between them. The most intense lines outline the magnetization blocking barrier (solid red lines).

Model of the exchange interaction in Dy_4 complex

The magnetic interactions between Dy^{III} ions include contributions from magnetic dipole−dipole and exchange interactions. The exchange coupling was simulated within the Lines model as described elsewhere.[5] Magnetic behavior of four interacting Dy^{III} ions was described using a noncollinear Ising Hamiltonian with one coupling constant:

$$\hat{H}_{exch} = -J\left(\hat{s}_{Dy_1}\hat{s}_{Dy_2} + \hat{s}_{Dy_1}\hat{s}_{Dy_1'} + \hat{s}_{Dy_1}\hat{s}_{Dy_2'} + \hat{s}_{Dy_2}\hat{s}_{Dy_1'} + \hat{s}_{Dy_2}\hat{s}_{Dy_2'} + \hat{s}_{Dy_1'}\hat{s}_{Dy_2'}\right)$$

(Eq. 1)

where s_i are projection operators of the effective spin of Dy^{III} ion on the corresponding anisotropy axis. J is the parameter of the inter-site magnetic exchange interaction and represents the only fitting parameters of the employed model. The inter-site magnetic dipole-dipole interaction is computed using Eq. (2) and added to the exchange Hamiltonian:

$$\hat{H}_{dip}(i,j) = \mu_{Bohr}^2 \times \frac{\hat{\mu}_i \cdot \hat{\mu}_j - 3(\hat{\mu}_i \cdot n_{ij})(\hat{\mu}_j \cdot n_{ij})}{r_{ij}^3}$$

(Eq. 2)

where $\hat{\mu}_i, \hat{\mu}_j$ are the magnetic moments on the sites i and j, respectively, as obtained from the SINGLE_ANISO single-site calculations, n_{ij} is the normalized vector connecting sites i and j (of length = 1), r_{ij} is the distance between magnetic sites i and j, while μ_{Bohr}^2 is the square Bohr magneton constant, with an approximate value of 0.4329702 cm^{-1}/Tesla. The total Hamiltonian of magnetic interaction is a sum of the two operators:

$$\hat{H}_{total} = \hat{H}_{exch} + \hat{H}_{dip}$$

(Eq. 3)

The low-lying energy spectra obtained by diagonalization of the $\hat{H}_{total}$ and of individual $\hat{H}_{exch}$ and $\hat{H}_{dip}$ are given in Table S8. The energy splitting gives a rough estimation on the importance of exchange and dipolar couplings on the total interaction. As such, for the considered Dy_4 the dipole-dipole interaction induces a weaker energy splitting compared to exchange interaction.

The eigenstates of $\hat{H}_{total}$ are further used for the description of magnetic susceptibility and molar magnetization of the entire tetranuclear compounds. The parameters J were found by minimization of the standard deviation function between measured and calculated magnetic susceptibility. Given that the exchange interaction is rather weak and induces weak splitting, only the low-temperature experimental data points, below 70 K, were considered in the fitting. This task was achieved within the POLY_ANISO code. The best fit gives the coupling value J = -0.24565 cm^{-1}.

Table S8 Energies of the lowest spin-orbit states (cm^{-1}).

Low-lying exchange states (cm^{-1})			
Exchange only	Dipole-dipole only	Total	Total, relative
-2.6411939	-0.8268643	-3.4747321	0.000000000
-2.6411939	-0.8268643	-3.4747321	0.000000000
-0.5406321	-0.5065744	-1.0485004	2.426231694
-0.5405842	-0.5065722	-1.0484983	2.426233849
-0.5403501	-0.5050773	-1.0483397	2.426392428
-0.5403020	-0.5050751	-1.0483375	2.426394586
-0.4692778	-0.0937192	0.3870260	3.861758241
-0.4692777	-0.0937191	0.3870260	3.861758243
0.4903774	-0.0224825	0.9630230	4.437755225
0.4903886	-0.0224824	0.9630384	4.437770638
0.4910579	0.4767332	0.9652786	4.440010783
0.4910691	0.4767530	0.9652943	4.440026494
1.1290081	0.4774673	1.1116337	4.586365877
1.1290081	0.4774870	1.1116340	4.586366194
1.8814458	0.8841908	1.8038297	5.278561938
1.8814458	0.8841908	1.8038297	5.278561951
…	…	…	…

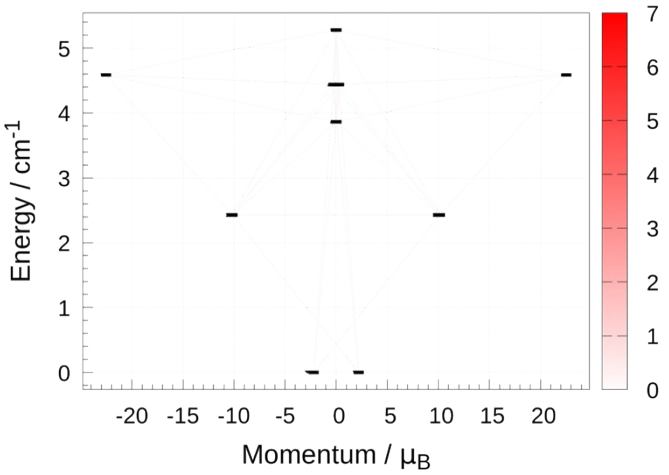

Fig. S14 Exchange magnetization blocking barrier for **Dy_4**. Each doublet state $\pm M_J$ arising from the magnetic coupling of the ground Kramers doublets on Dy^{III} ions. The intensity of the pink lines indicates the amplitude of the average transition magnetic dipole moment in μ_B between the connected states (see the legend in the right-hand side), the square of which roughly scales with the rate of spin-phonon transition between them. The most intense lines outline the magnetization blocking barrier (solid red lines). The almost incolor transition lines indicate that the relaxation within the exchange path is not effective: temperature-assisted relaxation is due to relaxation on individual ions, mainly Dy2 and Dy2'. The sites Dy1 and Dy1' define the relaxation barrier height in this compound.

References

[1] a) G. M. Sheldrick, A short history of SHELX, *Acta Crystallogr., Sect. A*, 2008, **64**, 112-122; b) *SHELXS-97 Program for Crystal Structure Solution*, University of Göttingen: Germany, 1997.

[2] O. V. Dolomanov, L. J. Bourhis, R. J. Gildea, J. A. K. Howard, H. Puschmann, OLEX2: a complete structure solution, refinement and analysis program, *J. Appl. Crystallogr.*, 2009, **42**, 339-341.

[3] E. A. Boudreaux, L. N. Mulay, *Theory and Applications of Molecular Paramagnetism*, John Wiley & Sons: New York, 1976.

[4] I. Fdez. Galván, M. Vacher, A. Alavi, C. Angeli, F. Aquilante, J. Autschbach, J. J. Bao, S. I. Bokarev, N. A. Bogdanov, R. K. Carlson, L. F. Chibotaru, J. Creutzberg, N. Dattani, M. G. Delcey, S. S. Dong, A. Dreuw, L. Freitag, L. M. Frutos, L. Gagliardi, F. Gendron, A. Giussani, L. González, G. Grell, M. Guo, C. E. Hoyer, M. Johansson, S. Keller, S. Knecht, G. Kovačević, E. Källman, G. Li Manni, M. Lundberg, Y. Ma, S. Mai, J. P. Malhado, P. Å. Malmqvist, P. Marquetand, S. A. Mewes, J. Norell, M. Olivucci, M. Oppel, Q. M. Phung, K. Pierloot, F. Plasser, M. Reiher, A. M. Sand, I. Schapiro, P. Sharma, C. J. Stein, L. K. Sørensen, D. G. Truhlar, M. Ugandi, L. Ungur, A. Valentini, S. Vancoillie, V. Veryazov, O. Weser, T. A. Wesołowski, P.-O. Widmark, S. Wouters, A. Zech, J. P. Zobel, R. Lindh, OpenMolcas: From Source Code to Insight, *J. Chem. Theory Comput.*, 2019, **15**, 5925-5964.

[5] M. E. Lines, Orbital Angular Momentum in the Theory of Paramagnetic Clusters, *J. Chem. Phys.*, 1971, **55**, 2977-2984.